



Article

Biosorption of Chromium (VI) in Aqueous Solution by Fermented Sweet Sorghum Residues: Kinetics, Isotherm and Mechanism

Jinling Wu ^{1,2,*}, Jing Dong ¹ and Xuan Guo ¹¹ Laboratory of Environmental Technology, INET, Tsinghua University, Beijing 100084, China² Beijing Key Laboratory of Radioactive Waste Treatment, Tsinghua University, Beijing 100084, China* Correspondence: jinlingwu@tsinghua.edu.cn; Tel.: +86-10-6279-6856

How To Cite: Wu, J.; Dong, J.; Guo, X. Biosorption of Chromium (VI) in Aqueous Solution by Fermented Sweet Sorghum Residues: Kinetics, Isotherm and Mechanism. *Environmental and Microbial Technology* **2026**, *1*(1), 6.

Received: 21 November 2025

Revised: 15 December 2025

Accepted: 30 December 2025

Published: 8 January 2026

Abstract: Fermented sweet sorghum residues (FSSR) were developed as an eco-friendly and low-cost biosorbent for the removal of chromium(Cr)(VI) from aqueous solutions, and their adsorption kinetics, isotherm and mechanism, and practical application potential were systematically investigated. The results showed that under the conditions of an initial Cr(VI) concentration of 50 mg/L, pH = 2.0, adsorbent dosage of 0.1 g, and temperature of 303 K, the equilibrium adsorption capacity (q_e) of FSSR for Cr(VI) reached 7.37 ± 0.44 mg/g, which was 61.6% higher than that of original sweet sorghum residues (SSR, 4.56 ± 0.19 mg/g); an independent-samples *t*-test confirmed that the difference was statistically significant ($p < 0.05$). Kinetic analysis revealed that Cr(VI) adsorption by FSSR followed the pseudo-second-order model ($R^2 > 0.91$; $k_2 = 0.021\text{--}0.079$ g/(mg·h)) and the Elovich model ($R^2 > 0.95$; $\alpha = 0.306\text{--}0.502$ mg/(g·h), $\beta = 0.625\text{--}1.010$ g/mg), indicating that chemisorption dominated the adsorption process, while equilibrium data were best described by the Freundlich isotherm model ($R^2 > 0.95$, $K_F = 0.83\text{--}4.76$ mg/g, $n = 2.01\text{--}3.64$), suggesting heterogeneous multi-layer adsorption. Advanced characterization techniques, including X-ray adsorption near-edge structure (XANES) and energy-dispersive spectroscopy (EDS), demonstrated a dual removal mechanism in which Cr(VI) was first reduced to Cr(III) on the surface of FSSR, followed by chemical adsorption of Cr(III). A comparison with biosorbents reported recently showed that FSSR exhibited competitive adsorption performance among the chemically modified biosorbents; although its maximum adsorption capacity was lower than that of some carbonized biosorbent, FSSR offers advantages in terms of cost-effectiveness and environmental sustainability, providing a feasible strategy for the valorization of agricultural residues and a sustainable alternative for the treatment of Cr(VI)-contaminated wastewater.

Keywords: sweet sorghum straw fermentation residue (FSSR); biosorption; heavy metal; chromium

1. Introduction

In recent years, increasing attention has been paid to the use of agricultural and forestry wastes, such as crop straw, as adsorbents for the removal of heavy metal ions [1]. Natural lignocellulosic materials are mainly composed of cellulose, hemicellulose and lignin [2,3]. Cellulose first forms microfibers, which then assemble into an ordered network skeleton of the fiber cell wall arranged in bundles. Hemicellulose is bonded to the surface of microfibers and forms a network through mutual connection, while lignin reinforces the cell walls, binds fibers, and connects



Copyright: © 2026 by the authors. This is an open access article under the terms and conditions of the Creative Commons Attribution (CC BY) license (<https://creativecommons.org/licenses/by/4.0/>).

Publisher's Note: Scilight stays neutral with regard to jurisdictional claims in published maps and institutional affiliations.

adjacent cells. Cellulose-hemicellulose or cellulose-lignin are connected by hydrogen bonds, whereas hemicellulose-lignin is connected by hydrogen bonds, ether bonds, ester bonds, etc. [4].

Chromium (Cr) is a kind of heavy metal. The main valence states of chromium are trivalent (Cr^{3+} , $\text{Cr}(\text{OH})_3^0$, $\text{Cr}(\text{OH})^{2+}$ and $\text{Cr}(\text{OH})_4^-$) and hexavalent (HCrO_4^- , CrO_4^{2-} , $\text{Cr}_2\text{O}_7^{2-}$). Hexavalent chromium (Cr(VI)), whose toxicity is three times that of Cr(III), is recognized as one of the most toxic heavy metal ions in aquatic environments, posing severe threats to ecological systems and human health due to its high solubility, mobility, and bioaccumulation potential [5,6]. For aquatic organisms, even trace concentrations of Cr(VI) ($\geq 0.05 \text{ mg/L}$) can disrupt cellular metabolism, induce oxidative stress, and cause irreversible damage to aquatic plants and invertebrates, ultimately disrupting the balance of aquatic food webs. For humans, long-term exposure to Cr(VI)-contaminated water (via drinking or skin contact) is closely associated with a significantly increased risk of chronic diseases, including kidney damage, respiratory inflammation, and even carcinogenesis (e.g., lung cancer and bladder cancer). Moreover, Cr(VI) can persist in groundwater and surface water for decades, with a half-life of up to 10 years in anaerobic environments, making its efficient removal from aqueous solutions an urgent priority for environmental remediation and public health protection. Unlike Zn, Pb and Cu, Cr exists in both cations and anions in aqueous solution. Therefore, its requirements for adsorbents are different from other metal cations.

Thabede et al. used black cumin seeds as adsorbent for Cr(VI) [7]. Adsorption capacity reached 10.15 mg/g. KMnO_4 and H_3PO_4 treated seeds featured higher adsorption capacities of 16.12 and 15.98 mg/g. Vinayagam et al. adsorbed Cr(VI) with sugarextracted marine algae with adsorption capacity of 6.41 mg/g [8]. Adsorption data conformed to Freundlich isotherm. Straw is the most common natural material. At present, straw of many plants was also used in the study of heavy metal ion adsorption [9–14]. Gkika reviewed the adsorbents extracted from biomass for adsorbing Cr(VI) [15]. Olive leaves Chemlali pruning waste had the highest adsorption efficiency of 99.98% [16]. Zhen et al. utilized mixed feedstocks to prepare a novel hydrochar adsorbent for trace amounts of Cr(VI) in acidic wastewater with adsorption capacity of 132 mg/g [17].

The study of adsorption mechanism helped adsorbent modification and adsorption system design. Biosorption of heavy metals is usually a complex process, which is the result of the comprehensive action of a variety of adsorption mechanisms and is controlled by a variety of influencing factors [18–21]. Common adsorption processes include complexation, coordination, ion exchange, diffusion, microprecipitation, electrostatic interaction and so on. Generally, the adsorption mechanism of agricultural and forestry waste adsorbents is mainly ion exchange and coordination complex mechanism. The natural materials contain K, Na, Ca and Mg ions, which provides conditions for the exchange of heavy metals. Ion exchange plays a major role in adsorption of natural materials. The surface of natural biomass materials is covered with hydroxyl, carboxyl, amino and methoxy. The nitrogen, oxygen and sulfur atoms in these functional groups contain lone pair electrons and have a good coordination effect on heavy metal ions. Therefore, coordination is also one of the most important mechanisms of biological adsorbents.

Cr(VI) adsorption is usually accompanied by redox reaction. Under acidic conditions, CrO_4^{2-} or $\text{Cr}_2\text{O}_7^{2-}$ reacts with H^+ to reduce to Cr(III). Reduction mechanisms usually include direct reduction mechanism and indirect reduction mechanism. In direct reduction, when Cr(VI) contacts the electron donor group with low reduction potential energy on the surface of the material, it is directly reduced to trivalent. In indirect reduction, Cr(VI) was connected to positively-charged functional groups electrostatic attraction, and then reduced to Cr(III) by adjacent electron donor, and finally was released or complexed with adjacent functional groups by electrostatic repulsion. Under acidic conditions, the reaction equations of CrO_4^{2-} or $\text{Cr}_2\text{O}_7^{2-}$ with H^+ are shown in Equations (1) and (2) respectively [22]. A large number of studies have proved reduction mechanism [23–27].



Sorghum is broadly planted in China. Sweet sorghum can adapt to a wide range of climatic conditions and can be planted from low temperature to tropical areas. The annual output in China is estimated to be 2,500,000 tons [28]. Due to its many advantages, sweet sorghum straw is widely used in fermentation for ethanol production. The fermented residues usually served as livestock feed or fertilizer. The previous research of our research group found that sweet sorghum straw residues (SSR) is an effective heavy metal adsorption material, especially the adsorption capacity of fermented sorghum straw residues (FSSR) for Cu(II) has been improved after fermentation [29]. In this work, FSSR served as an adsorbent to study another heavy metal chromium's adsorption, because Cr and Cu have different forms in water. The adsorption performance of FSSR for typical heavy metal anions were investigated together with its adsorption kinetics, isothermal adsorption and adsorption mechanism. This paper helped to effectively treat and repair the water polluted by heavy metals, provide a high-value application way for

agricultural and forestry waste, turn waste into treasure, and provide a theoretical basis for heavy metal wastewater treatment engineering.

2. Materials and Methods

2.1. Preparation of SSR and FSSR

The raw sweet sorghum residue (SSR) used in this experiment was obtained from the stalks of sweet sorghum harvested in farmlands of Changzhou, Hebei in China. After natural air-drying, impurities (such as leaves and soil particles) were removed. The pretreated stalks were crushed and then sieved through a standard 40-mesh sieve, and then dried at 60 °C for 24 h. The prepared SSR was sealed and stored in a desiccator for subsequent use.

Fermented sweet sorghum residue (FSSR) was prepared by ethanol fermentation of SSR via the traditional solid-state fermentation method. The residual straw residue was acidic, with impurities adhering to its surface; when immersed in water, it would leach organic substances and cause coloration. The residue was soaked and washed with water until neutralized, then dried at 60 °C and sieved through a 40-mesh sieve.

2.2. Chemical Reagents

$K_2Cr_2O_7$ was purchased from Tianjin Yongda Chemical Reagent Development Center (Tianjin, China). $NaOH$, HCl , H_2SO_4 were purchased from Beijing Chemical Plant (China). All were analytical reagents.

2.3. Adsorption Experiment

2.3.1. Preparation of Cr(VI) Stock Solution and Simulated Wastewater

Accurately weigh 2.8289 g of dried $K_2Cr_2O_7$ (dried at 110 °C for 2 h), dissolve it in a small amount of ultrapure water, transfer the solution into a 1000 mL volumetric flask, dilute to the mark with ultrapure water, and shake well to prepare a 1000 mg/L Cr(VI) standard stock solution. The simulated Cr(VI) wastewater with different concentrations used in the experiment was prepared by diluting the stock solution with ultrapure water, and its pH was adjusted with 0.1 mol/L HCl or 0.1 mol/L $NaOH$ solution.

2.3.2. Adsorption Kinetics Experiment

In a series of Erlenmeyer flasks, 0.1 g of FSSR or SSR adsorbent was added respectively, followed by the addition of 15 mL of simulated Cr(VI) wastewater with an initial concentration of 50 mg/L. The pH of the system was adjusted to 2.0, and the flasks were placed in a constant temperature shaking incubator at 30 °C (303.15 K) with a shaking speed of 150 r/min for adsorption experiments. Samples were taken at adsorption time of 0, 1, 2, 3, 4, 5, 6, 7, 8, 9, 10, 14, 15, 16, 17, 18, 19, and 24 h, respectively. After each sampling, the sample was centrifuged immediately at 5000 r/min for 5 min, and the supernatant was filtered through a 0.45 μ m organic filter membrane. The residual concentration of Cr(VI) in the filtrate was determined by 1,5-diphenylcarbazide spectrophotometry. Three parallel experiments were set up for each group, and the average value was taken as the final result.

2.3.3. Adsorption Isotherm Experiment

0.1 g of FSSR adsorbent was added to 100 mL of simulated Cr(VI) wastewater with initial concentrations of 25, 50, 75, 100, 150 and 200 mg/L respectively. The pH of the system was adjusted to 2.0, and the flasks were placed in constant temperature shaking incubators at 10 °C, 20 °C, 30 °C and 40 °C (283.15K, 293.15 K, 303.15 K, 313.15 K) for 24 h of adsorption (preliminary experiments confirmed that adsorption equilibrium was achieved at this time). After adsorption, the sample was centrifuged and filtered, the residual concentration of Cr(VI) in the filtrate was determined, and the equilibrium adsorption capacity q_e was calculated. Three parallel experiments were set up for each group, and the average value was taken as the final result.

2.3.4. Influence Factor Experiments

The initial concentration of Cr(VI) was fixed at 50 mg/L, the pH was 2.0, the temperature was 30 °C, and the adsorption time was 24 h. The adsorbent dosage was changed to 0.05, 0.1, 0.2, 0.3 and 0.4 g, respectively, to explore the effect of dosage on the adsorption capacity and removal rate. The adsorbent dosage was fixed at 0.1 g. The pH of the system was adjusted to 2.0, 3.0, 4.0, 5.0 and 6.0 respectively, to investigate the effect of pH on the adsorption performance. The initial pH was adjusted to 2.0, 3.0, 4.0, 7.0 and 10.0. The ionic strength of the solution was adjusted using sodium nitrate ($NaNO_3$). The adsorption capacity of the adsorbent was investigated at ionic

strengths of 0, 0.002, 0.02 and 0.2 mol/L, with the reaction being equilibrated for 24 h at a constant pH, to investigate the effect of ion strength.

2.4. Determination of Cr

The concentration of total Cr concentration in the supernatant was determined by Atomic Absorption Spectrophotometer (Analytik Jena Vario 6, Jena, Germany). The concentration of Cr(VI) was analyzed by diphenylcarbazide spectrophotometry.

2.5. Analysis of Interaction between Cr and FSSR

The material after Cr(VI) adsorption by FSSR was sampled for X-ray absorption near edge structure spectrum (XANES) determination after being ground into powder, sieved through 400 mesh, and then coated with adhesive tape. Typical metal anion Cr(VI) reference materials were selected as $K_2Cr_2O_7$, $KCrO_4$, CrO_3 , Cr_2O_3 , $CrCl_3$, $Cr_2(SO_4)_3$ and $Cr(NO_3)_3$. The XANES experiment was carried out through the synchrotron radiation facility (Institute of High Energy Physics, Chinese Academy of Sciences, Beijing). The reference sample was measured in transmission mode. The Cr adsorbed FSSR (Cr-FSSR) sample was measured in fluorescence mode. The spectrum was solved by software IFEFFIT.

Scanning electron microscope- energy-dispersive spectroscopy (SEM-EDS) was analyzed by Field Emission Scanning Electron Microscope (FEI Quanta 200 ESEM FEG, Eindhoven, The Netherlands)

2.6. Data Processing

All experimental data were sorted out and plotted by Origin 2021 software. The adsorption kinetics data were fitted by pseudo-first-order kinetic model (PFO) and pseudo-second-order kinetic model (PSO) and Elovich models [30,31]; the adsorption isotherm data were fitted by Langmuir, Freundlich, Temkin and Redlich Peterson (R-P) isotherm models [32,33]. Statistical analysis was performed, and the independent-samples *t*-test was used to verify the significant difference in adsorption performance between FSSR and SSR (*p* < 0.05 was considered statistically significant).

3. Results and Discussion

3.1. Adsorption Kinetics

The initial concentration was set as 50 mg-Cr/L in reaction solution, which was prepared with $K_2Cr_2O_7$. The initial pH is 2.0, and the temperature is 30 °C. FSSR and SSR weighed 0.1 g respectively. The Cr adsorption content with contact time was shown in Figure 1. The adsorption of Cr by FSSR and SSR were both slower than that of Cu [29]. The adsorption equilibrium was reached in more than 18 h. We proposed that the adsorption equilibrium was completely achieved at 24 h, and statistical analysis *t*-test was performed on the results of three parallel adsorption experiments at this time point. The equilibrium Cr(VI) adsorption capacity of FSSR (7.37 ± 0.44 mg/g) was significantly higher than that of raw SSR (4.56 ± 0.19 mg/g) (*t* = 11.24, *df* = 4, *p* < 0.01, independent-samples *t*-test). The equilibrium total Cr adsorption capacity of FSSR (2.81 ± 0.19 mg/g) was significantly higher than that of SSR (2.35 ± 0.08 mg/g) (*t* = 5.79, *df* = 4, *p* < 0.01, independent-samples *t*-test). These results confirm that FSSR has remarkably superior both Cr(VI) and total Cr removal performance compared with SSR. At the same time, for both FSSR and SSR the *q_t* values of Cr(VI) were higher than those of total Cr. It indicated that the reduction reaction occurred during adsorption, by which hexavalent chromium was reduced to trivalent which remained in solution. Lignin in the adsorbent contained phenolic hydroxyl and other reducing functional groups, which could reduce the oxidized Cr(VI) to Cr(III). Cr^{3+} is a cation and cannot be adsorbed by protonated materials at low pH. Cr mainly exist in the following forms: $Cr(OH)_4^-$, $Cr(OH)_3^0$, $Cr(OH)_2^+$, Cr^{3+} , $Cr_2O_7^{2-}$, CrO_4^{2-} and CrO_4^- at different pH of the solution [34].

Form distribution of hexavalent and trivalent chromium is shown in Figure 2. The main existing forms of hexavalent chromium ions in the solution are CrO_4^{2-} , $HCrO_4^-$, $Cr_2O_7^{2-}$ and H_2CrO_4 (aq). The main existing forms of trivalent chromium ions in the solution are $Cr(OH)_3$ (aq), $Cr(OH)_2^+$, Cr^{3+} and $Cr_2(OH)_2^{4+}$. When the pH value was less than 5.0, the main existing forms were anionic $HCrO_4^-$ and cationic Cr^{3+} . When the solution was acidic, the adsorbent surface was protonated and therefore repelled the cations. The optimum pH for Cr(VI) was different from Cr(III). The low adsorption capacity of total chromium ions at the optimal pH for Cr(VI) was resulted from the optimum adsorption capacity of Cr(VI) and Cr(III) unable to reach at the same time.

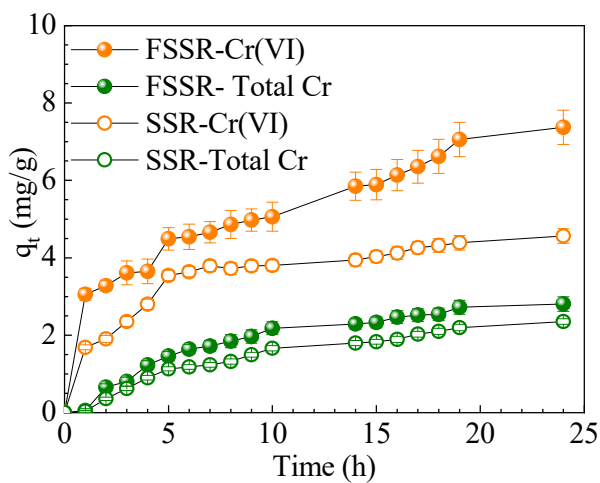


Figure 1. Cr adsorption by FSSR and SSR (q_t : adsorption capacity (mg/g)).

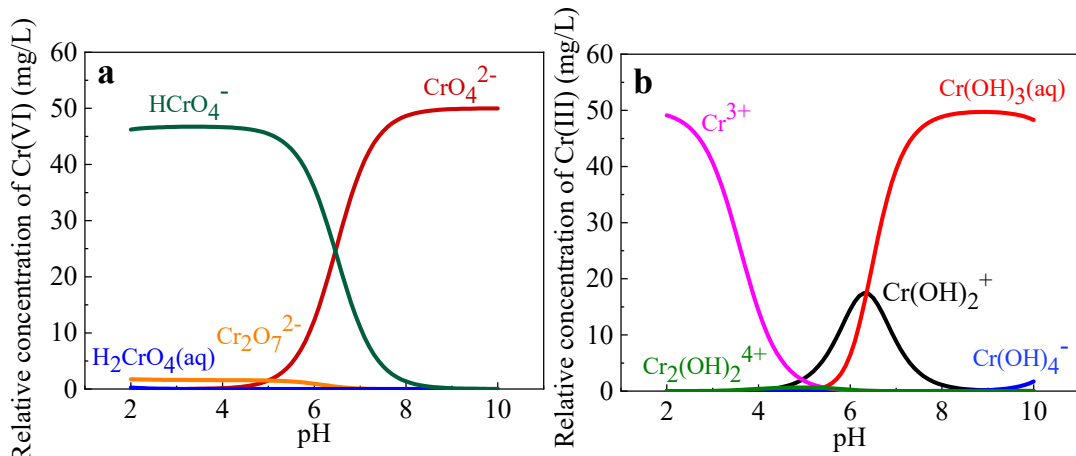


Figure 2. Distribution of (a) Cr(VI) and (b) Cr(III) in the solution of 50 mg-Cr/L.

The experimental data of FSSR and SSR adsorbing hexavalent and total chromium were fitted with PFO, PSO and Elovich models in this study (Figure 3). The fitted kinetic parameters are shown in Table 1. Adsorption data of FSSR and SSR for Cr fit Elovich kinetic model well with the correlation coefficients all higher than 0.95, which indicated that the adsorption reaction was chemical adsorption and heterogeneous adsorption. Due to the Cr(VI) reduction reaction, the initial adsorption rate constants of Cr(VI) (α) were higher than those of total Cr for both FSSR and SSR. In addition, the fitting results of PSO model for SSR were good indicating a chemical reaction process as well.

Table 1. Fitting data of kinetic models for FSSR and SSR.

FSSR		SSR	
Cr(VI)	Total Cr	Cr(VI)	Total Cr
Pseudo first-order kinetics			
k_1	0.226 ± 0.020	0.130 ± 0.032	0.307 ± 0.040
q_e	6.44 ± 0.16	2.86 ± 0.29	4.22 ± 0.14
R^2	0.861	0.986	0.966
Pseudo second-order kinetics			
k_2	0.038 ± 0.005	0.028 ± 0.012	0.079 ± 0.016
q_e	7.56 ± 0.23	3.92 ± 0.50	4.90 ± 0.19
R^2	0.916	0.984	0.977
Elovich kinetics			
α	4.730 ± 0.679	0.502 ± 0.101	4.450 ± 1.070
β	0.625 ± 0.036	0.818 ± 0.140	1.010 ± 0.085
R^2	0.959	0.979	0.968

k_1 : PFO adsorption kinetic constant (1/h); k_2 : PSO adsorption kinetic constant (g/(mg·h)); q_e : adsorption capacity at equilibrium (mg/g); α : initial adsorption rate (mg/(g·h)); β : desorption constant in Elovich Model (g/mg); TC: total Cr.

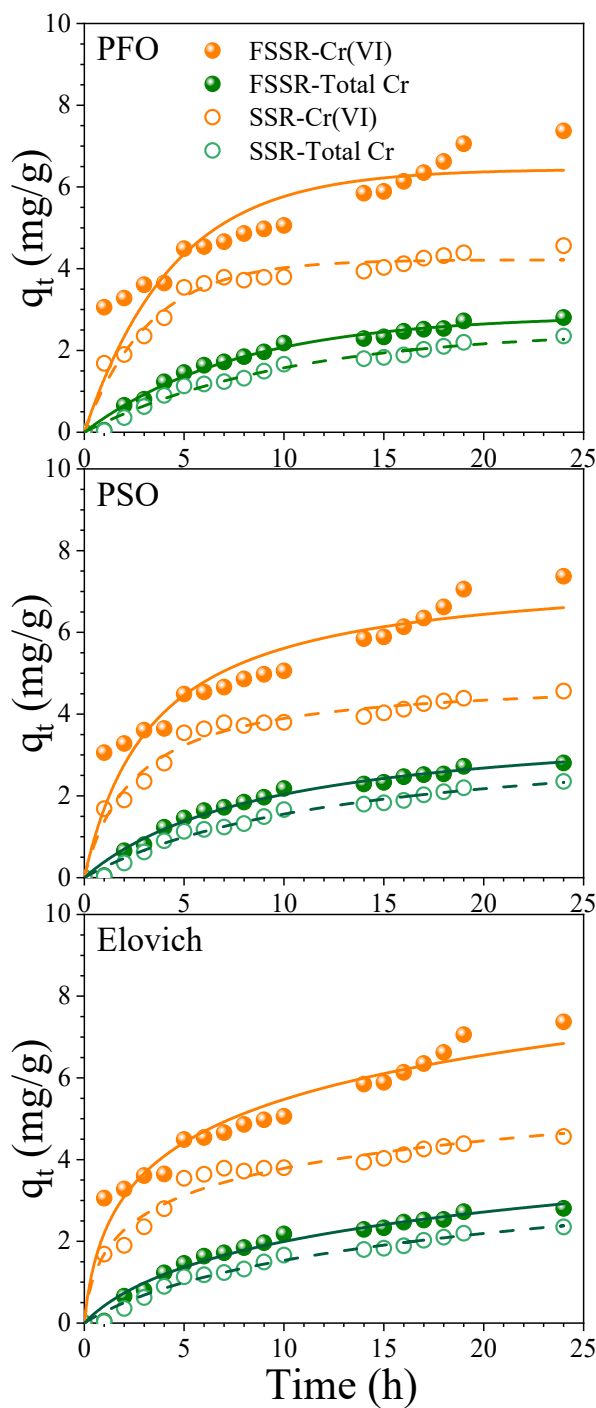


Figure 3. The kinetic fitting curves of Cr adsorption by FSSR and SSR.

3.2. Adsorption Isotherm

The isothermal adsorption processes by FSSR at different temperatures were studied with adsorbent weight of 0.1g, initial pH of 2.0 and the reaction time of 24h. The reaction solution was prepared with $K_2Cr_2O_7$ with the initial concentrations of chromium ion as 25, 50, 75, 100, 150, 200 and 250 mg/L respectively. The results are shown in Figure 4. The data were simulated by Langmuir, Freundlich, Temkin and R-P models (Figures 5 and 6, Tables 2 and 3).

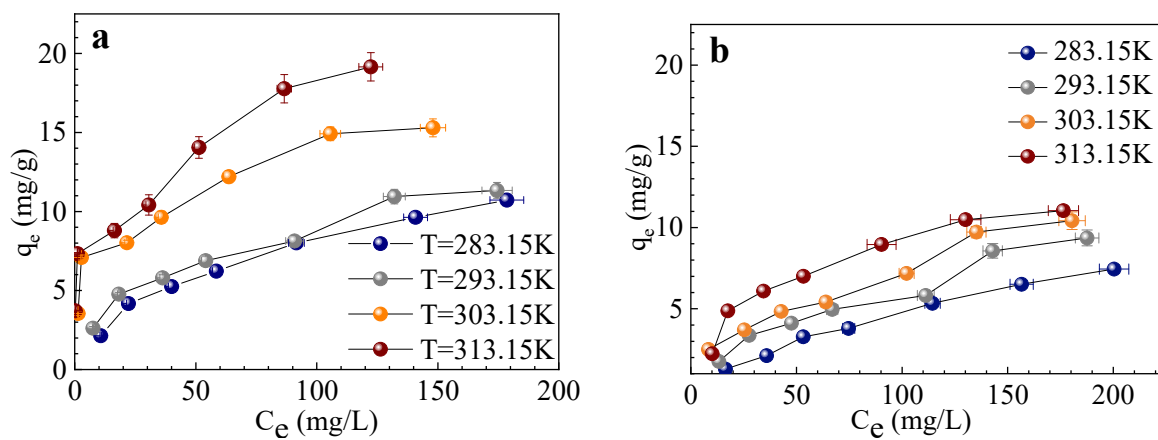
Table 2. Adsorption isothermal parameters for Cr(VI) by FSSR.

Model	Temperature (K)			
	283.15	293.15	303.15	313.15
Langmuir				
q_m (mg/g)	14.3 ± 4.4	13.9 ± 3.4	13.5 ± 1.2	23.0 ± 3.4
K_L (L/mg)	0.015 ± 0.011	0.021 ± 0.014	0.219 ± 0.115	0.035 ± 0.016
R^2	0.992	0.969	0.859	0.813
Freundlich				
K_F (mg/g)	0.83 ± 0.31	1.20 ± 0.38	3.90 ± 0.56	4.76 ± 0.57
n	2.01 ± 0.33	2.28 ± 0.36	3.64 ± 0.44	3.56 ± 0.37
R^2	0.995	0.989	0.966	0.952
Temkin				
A (L/g)	0.168 ± 0.086	0.283 ± 0.165	3.95 ± 3.01	16.3 ± 12.0
B (J/mol)	342 ± 73	382 ± 80	486 ± 78	523 ± 66
R^2	0.980	0.950	0.892	0.822
R-P				
K_{RP} (L/g)	0.423 ± 0.878	3.65 ± 40.70	-	-
α_{RP} (L/mg) ^β	0.188 ± 0.876	2.66 ± 33.80	-	-
β_{RP}	0.673 ± 0.457	0.584 ± 0.267	-	-
R^2	0.997	0.989	-	-

q_m : theoretical saturated adsorption capacity; K_L : adsorption equilibrium constant; K_F : Freundlich constant; n : a parameter in the Freundlich model; A : a constant in Temkin model; B : the change of adsorption energy in the Temkin model; K_{RP} : isothermal adsorption constant in R-P model; α_{RP} : a parameter in R-P model; β_{RP} : an index between 0 and 1 in R-P model.

Table 3. Adsorption isothermal parameters for total Cr by FSSR.

Model	Temperature (K)			
	283.15	293.15	303.15	313.15
Langmuir				
q_m (mg/g)	15.2 ± 4.1	15.6 ± 2.6	15.9 ± 2.0	13.5 ± 0.9
K_L (L/mg)	0.005 ± 0.002	0.007 ± 0.002	0.0104 ± 0.002	0.024 ± 0.004
R^2	0.998	0.960	0.976	0.986
Freundlich				
K_F (mg/g)	0.20 ± 0.07	0.39 ± 0.10	0.63 ± 0.13	1.28 ± 0.18
n	1.46 ± 0.16	1.65 ± 0.14	1.85 ± 0.15	2.35 ± 0.17
R^2	0.996	0.974	0.986	0.996
Temkin				
A (L/g)	0.077 ± 0.022	0.115 ± 0.031	0.200 ± 0.061	0.233 ± 0.065
B (J/mol)	405 ± 61	383 ± 49	418 ± 50	380 ± 40
R^2	0.987	0.889	0.928	0.975
R-P				
K_{RP} (L/g)	0.09 ± 0.08	-	-	-
α_{RP} (L/mg) ^β	0.03 ± 0.19	-	-	-
β_{RP}	0.7 ± 0.8	-	-	-
R^2	0.998	-	-	-

**Figure 4.** Adsorption isotherm of (a) Cr(VI) and (b) total Cr by FSSR (C_e : Cr concentration at equilibrium (mg/L)).

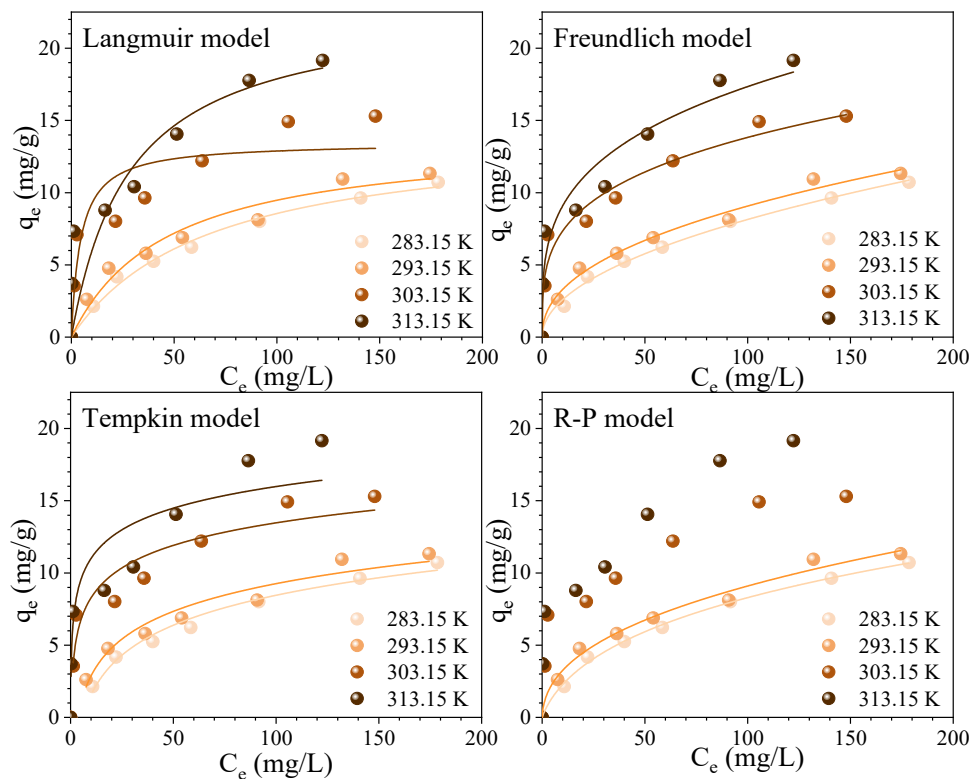


Figure 5. Adsorption isotherm modelling for Cr(VI) by FSSR.

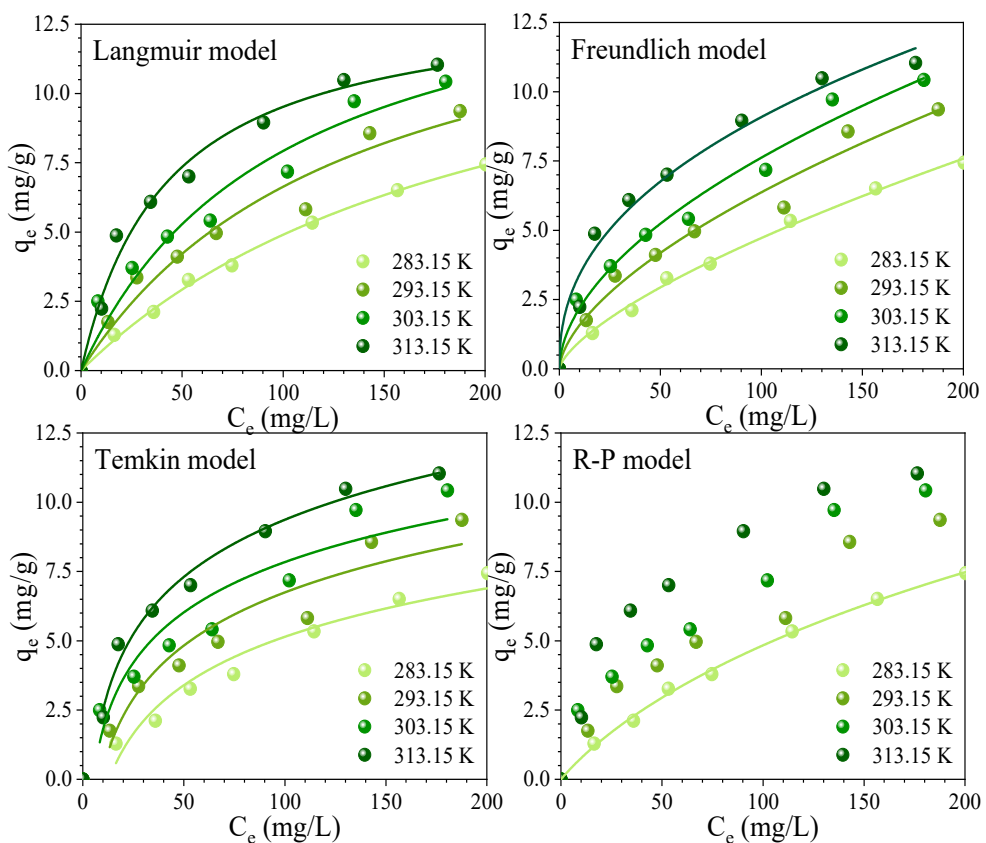


Figure 6. Adsorption isotherm modelling for total Cr by FSSR.

With the increase of temperature (Figure 4), the adsorption capacity of FSSR for Cr(VI) increased significantly. When the temperature increased from 283.15 to 313.15 K, the adsorption capacity increased from 14.29 to 20.41 mg/g by nearly 50%. The adsorption capacity of total chromium ions was much lower than that of Cr(VI), indicating that part of Cr(VI) was converted to Cr(III), which still existed in the solution during the removal process of Cr(VI).

The experimental data fit the Freundlich isothermal adsorption model the best among the four isotherms with the correlation coefficient R^2 greater than 0.95 for both FSSR and SSR. It indicated that the adsorption process was limited by the adsorption sites, the adsorption sites of Cr on the adsorbent surface were uneven, and the adsorption capacity increased with the increase of concentration. When the adsorption sites were saturated, the adsorption rate gradually decreased and the adsorption capacity reached equilibrium. This was different from the fitting effect of Cu(II) adsorption on FSSR [29], which fit Langmuir model the best.

In terms of model fitting degree, the isotherm data of Cr(VI) and total Cr adsorption onto FSSR showed the best fitting effect with the Freundlich model ($R^2 = 0.952\sim0.995$ for Cr(VI), $R^2 = 0.974\sim0.996$ for total Cr, respectively), followed by the Langmuir model ($R^2 = 0.960\sim0.998$ just for total Cr adsorption). The fitting coefficients of the Langmuir model for Cr(VI) and the Temkin for both were low ($R^2 < 0.90$). The fitting of the Redlich-Peterson (R-P) model even exhibited non-convergence, which further indicates that the R-P model is not applicable to describe the Cr(VI) and total Cr adsorption onto FSSR. The fitting effect of Cr(VI) and total Cr adsorption on FSSR was different from that of Cr(II) adsorption, which fit Langmuir model the best.

The core assumption of the Freundlich model is that the adsorbent surface is heterogeneous, with active sites distributed unevenly in terms of energy, and the adsorption process is multi-layer adsorption with interactions between adsorbate molecules. The optimal fitting effect of this model in the study indicates that FSSR as biomass-based adsorbents, possess various types of active functional groups (e.g., carboxyl, hydroxyl and amino groups) on their surfaces. These functional groups exhibit different affinities for Cr(VI), leading to a non-uniform distribution of adsorption sites. Meanwhile, it suggests that the adsorption process is not limited to monolayer adsorption; after the high-affinity sites on the adsorbent surface are occupied by Cr(VI), subsequent adsorbate molecules can be further adsorbed onto the formed molecular layers or bind to low-affinity sites, which is highly consistent with the typical adsorption characteristics of biomass materials.

Notably, the Langmuir model ranks second in fitting effect for total Cr, indicating that monolayer adsorption on a homogeneous surface acts as a secondary adsorption mechanism for total Cr adsorption. The Langmuir model assumes a homogeneous adsorbent surface with active sites of uniform energy and no interactions between adsorbate molecules. Its relatively good fitting degree demonstrates that there are still some active sites with uniform energy on the surfaces of FSSR, where ordered monolayer adsorption of Cr, which was most likely Cr³⁺ because Cr(VI) does not conform to the Langmuir adsorption model.) occurs. Combined with the fitting priority of the two models, it can be concluded that the adsorption of Cr(VI) is a simple process dominated by heterogeneous multi-layer adsorption, however the adsorption of total Cr onto FSSR is a hybrid process dominated by heterogeneous multi-layer adsorption and supplemented by homogeneous monolayer adsorption.

The relatively poor fitting effects of the Temkin and R-P models also have clear physical implications. The Temkin model takes into account the interactions between adsorbate and adsorbent, assuming that the adsorption heat decreases linearly with the increase of adsorption capacity. Its low fitting coefficient suggests that the interaction strength between Cr(VI) and the adsorbent surface is relatively stable, or the variation of adsorption heat does not follow an obvious linear pattern. The R-P model is a hybrid form of the Langmuir and Freundlich models, which can be used to determine whether the adsorption is monolayer or multi-layer. Its poor fitting degree further confirms that the adsorption process is more inclined to the multi-layer heterogeneous adsorption described by the Freundlich model, rather than the transitional adsorption that the R-P model is more suitable for.

In terms of parameter values, the constant n in the Freundlich model reflects the ease of the adsorption process. In this study, the n values of Cr(VI) and total Cr were higher than 2.01 and 1.48, respectively, both greater than 1, indicating that the adsorption of Cr(VI) and total Cr onto both adsorbents is a favorable adsorption process that proceeds easily. Moreover, the higher n value at higher temperature indicates high temperature facilitates the adsorption reaction for both Cr(VI) and total Cr. The higher n value for Cr(VI) than total Cr implies that the adsorption reaction of Cr(VI) is more facile than that of total Cr. The Freundlich constant K_F is positively correlated with adsorption capacity; the K_F value of Cr(VI) (0.83–4.76 mg/g) is significantly higher than that of total Cr (0.20–1.28 mg/g), which directly demonstrates the higher adsorption capacity of Cr(VI) than that of total Cr. The maximum adsorption capacity q_m of total Cr fitted by the Langmuir model was 15.9 ± 2.0 mg/g at 303.15K. The optimal conditions for Cr(VI) adsorption by FSSR were initial Cr(VI) concentration of 50 mg/L, pH of 2.0, adsorbent dosage of 0.1 g and temperature of 313 K, under which the highest q_m of 23.0 ± 3.4 mg/g was achieved by Langmuir model.

3.3. Influencing Factors on Cr Adsorption

3.3.1. Adsorbent Dosage

Adsorption capacities of FSSR for Cr(VI) and total Cr (Figure 7a) both decreased slightly with FSSR dosage increasing from 0.05 to 0.10 g. With FSSR dose continuously increasing, the adsorption capacity decreased rapidly. The optimal FSSR dose was 0.1 g where the Cr(VI) adsorption capacity and the total Cr adsorption capacity reached 7.37 and 2.81 mg/g respectively. The q_e value of Cr(VI) was significantly higher than that of the total Cr, which was mainly due to Cr(VI) reduced by the reducing functional groups such as lignin or phenolic hydroxyl in FSSR. The reduction product Cr(III) remained in water instead of being adsorbed, resulting in low adsorption capacity of total Cr.

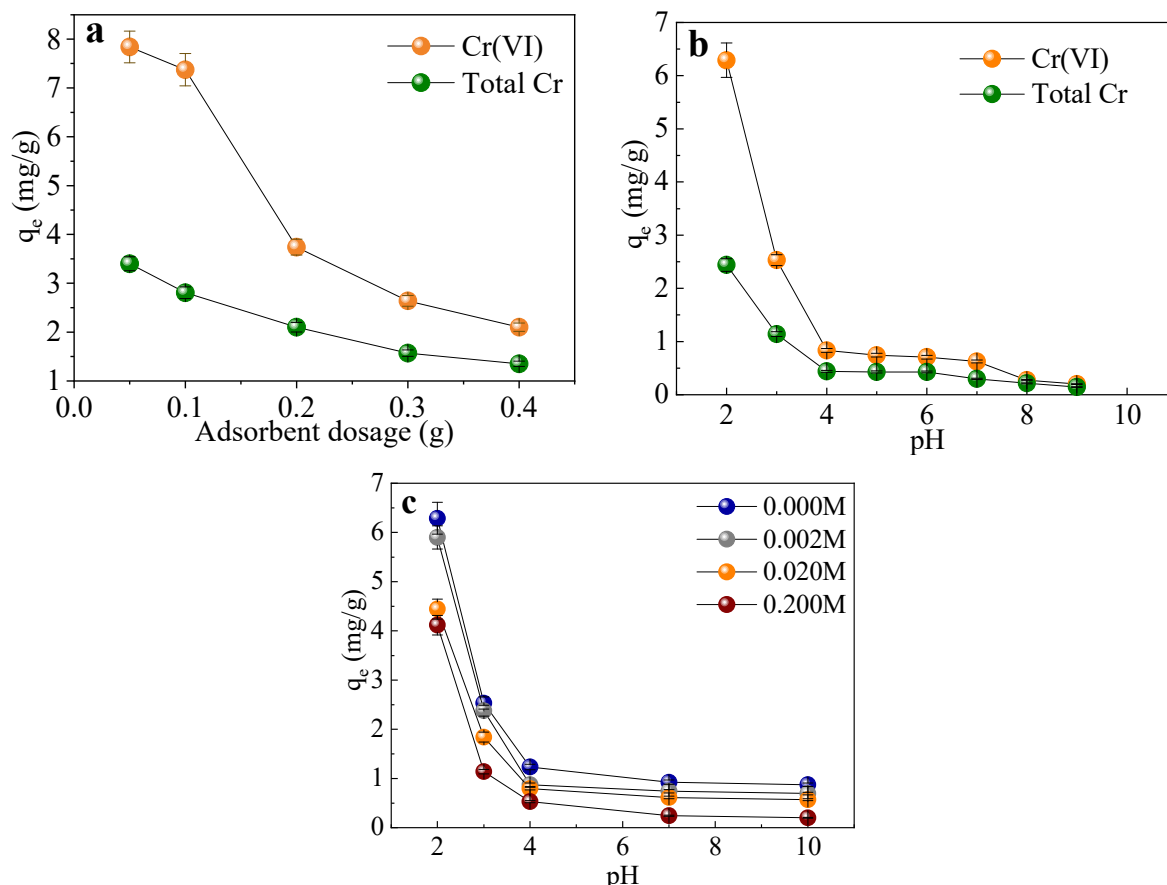


Figure 7. Influencing factors of Cr(VI) adsorption by FSSR: (a) adsorbent dosage, (b) initial pH on Cr and (c) ionic strength.

3.3.2. Initial pH

The optimal pH value for Cr(VI) removal biosorption was 2.0 (Figure 7b), where the equilibrium concentration of Cr(VI) detected in the solution was the lowest and therefore the maximum q_e value for Cr(VI) reached 7.3 mg/g at equilibrium. The q_e value decreased rapidly with pH increasing. pH had an important impact on the removal of chromium. The optimal pH for Cr(III) cations was more than 5.0. The q_e value of total chromium in acidic solution was significantly lower than the q_e value of Cr(VI). Therefore, the optimal pHs for Cr(VI) and Cr(III) adsorption were different, which could not be acquired at the same time.

3.3.3. Ion Strength

The q_e value was related to the initial pH and ionic strength (Figure 7c). At the same initial pH, high ionic strength resulted in low value of q_e . When the initial pH was higher than 4, the q_e value was relatively low and almost unaffected by the ionic strength. At pH of 2.0, the q_e value was the highest and significantly affected by ionic strength. At this time, the ionic strength not greater than 0.002 M had no obvious effect on the adsorption capacity. When the ionic strength increased to 0.2 M, and the adsorption capacity was 34.54% lower than that of the control sample.

3.4. Characterization of Interaction between FSSR and Cr

3.4.1. XANES

The normalized XANES spectrums of reference and sample are shown in Figure 8. Among them, three Cr(VI) references are $K_2Cr_2O_7$, $KCrO_4$ and CrO_3 respectively, five Cr(III) references are $Cr(CH_3COO)_3$, Cr_2O_3 , $CrCl_3$, $Cr(NO_3)_3$ and $Cr_2(SO_4)_3$ respectively. The top curve is Cr-FSSR. The peak positions of Cr(VI) reference, Cr(III) reference and zero valent chromium metal are obviously different. For Cr(VI) reference compounds ($K_2Cr_2O_7$, $KCrO_4$ and CrO_3), a distinct pre-edge feature was observed at approximately 5990–5995 eV, which is characteristic of tetrahedrally coordinated Cr(VI). In contrast, Cr(III) reference compounds exhibited no pronounced pre-edge peak and showed their main absorption edge at higher energies, consistent with octahedral Cr(III) coordination. The absorption peaks of Cr-FSSR were almost the same as those of the trivalent chromium reference without pre-edge peak around 5990–5995 eV before the main peak, which indicated that the trivalent chromium Cr(III) was adsorbed to FSSR surface. Zheng et al. also reported that trivalent chromium Cr(III) was able to adsorb on the seaweed [35].

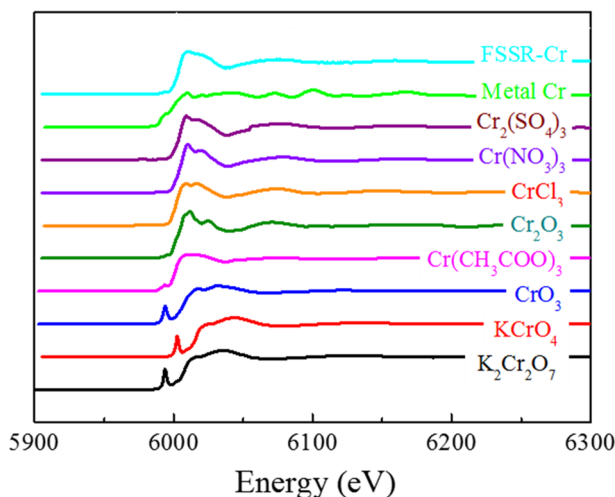


Figure 8. Normalized XANES spectra of reference and sample: $K^2Cr_2O_7$, $KCrO_4$, CrO_3 , $Cr(CH_3COO)_3$, Cr_2O_3 , $CrCl_3$, $Cr(NO_3)_3$, $Cr_2(SO_4)_3$, metal Cr, FSSR-Cr.

3.4.2. EDS

From EDS analysis of FSSR, the material surface was accumulated by cations including Na^+ , K^+ , Mg^{2+} , Ca^{2+} before adsorption. After adsorption, Cr elements were found on FSSR.

3.5. Proposed Mechanisms of Adsorption of Cr(VI) on FSSR

According to the results of static adsorption test, it was found that hexavalent chromium was reduced to trivalent chromium, which increased Cr(III) concentration in the solution. According to the XANES characterization results, it was found that there was only trivalent and no hexavalent chromium on the adsorbent surface. According to our previous work [29], after fermentation, the structure of cellulose changes and the number of active functional groups such as hydroxyl groups increases, making it easier for FSSR to biosorb metal cations. From EDS results, Cr cations and other metal cations were accumulated on FSSR which confirmed our previous work [29] and indicated the adsorption of Cr(III) cations. The mechanism of adsorption of Cr by FSSR is therefore proposed in this study: (1) Cr(VI) is reduced to Cr(III) under the existence of FSSR; (2) Cr(III) is directly biosorbed by FSSR due to the change of cellulose structure and the increase in functional groups such as hydroxyl groups in FSSR after fermentation.

Here we compared the proposed mechanism with Verma's study [36], because they also proposed the mechanism of Cr adsorption by cellulose organics. Verma reported the mechanism of coconut shell adsorbing Cr. He proposed that hexavalent chromium ions were first adsorbed to the organic functional groups on coconut shell, and then the main components in the adsorbent, such as hemicellulose, cellulose and lignin, were oxidized to reduce Cr(VI) and then form ether, carboxyl and other carbonyl functions. Cr(VI) itself was reduced to trivalent. It is consistent with the mechanism (1) of this study. However, there is no clear evidence of which parts and functions of cellulose, hemicellulose or lignin realize the reduction of Cr(VI). Verma also found that Cr(III) precipitated as $Cr(OH)_3$ in the adsorbent pore. This was related to the mechanism (2) proposed in this study, and

the interaction between hydroxyl and Cr(III) is proposed, but in this study the formation of Cr(OH)₃ precipitation was not found.

3.6. Limitations and Future Perspectives

Compared with recently reported biosorbents (Table 4), the FSSR material exhibits a competitive Cr(VI) adsorption capacity under acidic conditions, while simultaneously enabling partial reduction of Cr(VI) to Cr(III). Although some modified materials (mainly some adsorbents of biochar after carbonization, e.g., Defatted BCS, PBCKOH and hydrochar adsorbent) show higher adsorption capacities, FSSR offers advantages in terms of simple preparation, renewable feedstock utilization, and environmental friendliness, making it suitable for treating acidic chromium-containing effluents.

Table 4. Comparison of Cr(VI) adsorption performance of various biosorbents.

Adsorbent	Raw Material	pH	q _m (mg/g)	Mechanism	Ref.
KMnO ₄ or H ₃ PO ₄ treated BCS	Black cumin seeds (BCS)	1	15.98–16.12	Electrostatic attraction	[7]
Defatted BCS using acetone and DMF	Black cumin seeds		87.44	Surface area enhancement	[7]
Sugarextracted marine algae	Ulva prolifera	5.4	6.41	Multi-layer adsorption	[8]
PBCKOH (biochar)	Corn straw		116.97	Electrostatic attraction, complexation, ion exchange and reduction reaction	[12]
Olive leaves Chemlali pruning waste	Olive leaves	3.9	21.16–40.31	Carboxylic acid, hydroxyl and amide	[16]
Hydrochar adsorbent	Mixed feedstocks	Acidic	43.2–132	-NH ₃ ⁺ and carbonyl groups	[17]
FSSR	Sweet sorghum residue	2	13.5–23.0	Reduction reaction and chemical adsorption	This study

This work has certain limitations that need to be acknowledged. First, the maximum adsorption capacity of the adsorbent (13.5–23.0 mg/g) is relatively moderate compared with the advanced carbonized biosorbents reported in recent studies. This is mainly attributed to the relatively low specific surface area and limited number of active adsorption sites on the material surface. Second, the optimal adsorption process requires a high-acidity condition (pH 2.0), which restricts its direct application in neutral or alkaline wastewater treatment systems. Although the acidic condition can enhance the protonation of active groups and promote the adsorption of target pollutants via ion exchange, the need for pH adjustment will increase the operational cost in practical engineering.

However, it should be noted that our adsorbent has unique advantages that compensate for the above shortcomings, including extensive sources of raw materials, low cost of agricultural waste, simple, green and pollution-free preparation process and relative high selectivity to Cr(VI). In view of the high-acidity requirement, we propose that this adsorbent is more suitable for specific scenarios such as acidic industrial wastewater treatment (e.g., metal plating wastewater, mining wastewater), where the inherent acidic environment can directly match the optimal pH condition of the adsorption process, thus avoiding the additional cost of pH adjustment. To address the moderate adsorption capacity, we will optimize the material modification strategy in future work (e.g., introducing functional groups, increasing specific surface area via pore-forming modification).

Future research will focus on the following aspects to overcome the above limitations: (1) Selectivity enhancement and structural optimization of the biosorbent: Modification strategies such as chemical grafting of high-affinity functional groups, composite with porous materials will be adopted to increase the specific surface area and active sites, thereby improving the adsorption capacity. (2) Application potential of the prepared biosorbent: Valuated long-term stability, biosorbent regeneration, untested multi-metal systems, adsorption performance under neutral/alkaline conditions will be addressed in future work (3) Simulated and real wastewater treatment: For acidic industrial wastewater (e.g., mining wastewater containing heavy metals), long-term adsorption experiments will be carried out to verify the feasibility of practical application and optimize the process parameters.

4. Conclusions

This study developed fermented sweet sorghum residues (FSSR) as an eco-friendly, low-cost biosorbent for Cr(VI) removal from aqueous solutions, and systematically investigated its adsorption performance, mechanism, and practical application potential. Key findings are as follows: (1) Under the conditions of initial Cr(VI) concentration = 50 mg/L, pH = 2.0, adsorbent dosage = 0.1 g, temperature = 303 K, the equilibrium adsorption capacity (q_e) of FSSR for Cr(VI) reached 7.37 ± 0.44 mg/g, which was 61.6% higher than that of original sweet sorghum residues (4.56 ± 0.19 mg/g). Independent-samples t-test confirmed a statistically significant difference in

adsorption capacity between FSSR and SSR ($p < 0.05$). (2) Kinetic analysis revealed that the adsorption of Cr(VI) by FSSR followed the pseudo-second-order model ($R^2 > 0.91$, rate constant $k_2 = 0.021\text{--}0.079 \text{ g}/(\text{h}\cdot\text{mg})$) and Elovich model ($R^2 > 0.95$, $\alpha = 0.306\text{--}0.502$, $\beta = 0.625\text{--}1.010$), while equilibrium data were best fitted by the Freundlich isotherm model ($R^2 > 0.95$, $K_F = 0.83\text{--}4.76 \text{ mg/g}$, $n = 2.01\text{--}3.64$), indicating multi-layer chemisorption as the dominant mechanism. (3) Advanced characterizations (XANES and EDS) verified a dual removal mechanism: Cr(VI) was first reduced to Cr(III) on FSSR's surface, followed by chemical adsorption of Cr(III) onto FSSR. (4) Comparative analysis with biosorbents reported during 2021–2026 showed that FSSR exhibited superior performance (q_m) among the chemically modified biosorbents. Despite a lower q_m than some carbonized biosorbent, FSSR exhibited cost-effectiveness and broader pH adaptability.

FSSR proves a low-cost, eco-friendly Cr(VI) adsorbent, and its fermentation modification paves the way for green biomass adsorbent development. Limitations (unevaluated long-term stability/regeneration, untested multi-metal systems) will be addressed in future work (e.g., optimizing dilute HCl regeneration, testing simulated industrial wastewater). Overall, FSSR holds promise for low-concentration Cr(VI) wastewater treatment, and its modification technology provides a sustainable solution for high-performance biosorbents.

Author Contributions

J.W.: writing, methodology, investigation, data curation, supervision; J.D.: investigation, methodology, data curation; X.G.: data curation, software. All authors have read and agreed to the published version of the manuscript.

Funding

This research was funded by the National Key Research and Development Program (2016YFC1402507).

Institutional Review Board Statement

Not applicable.

Informed Consent Statement

Not applicable.

Data Availability Statement

The raw data used in this study can be obtained from the authors upon reasonable request. The authors will ensure the accessibility of these data to qualified professionals for at least 10 years following the publication of this paper.

Conflicts of Interest

The authors declare no conflict of interest.

Use of AI and AI-Assisted Technologies

No AI tools were utilized for this paper.

Nomenclature

A	A constant in the Temkin model (L/g)
B	The change of adsorption energy in the Temkin model (J/mol)
BCS	Back cumin seeds
C_e	The equilibrium concentration (mg/L)
df	Degrees of freedom
EDS	Energy dispersive spectroscopy
FSSR	Fermented sweet sorghum residues
k_1	The pseudo first-order adsorption kinetic constant (1/h)
k_2	The pseudo second-order adsorption kinetic constant (g/(mg·h))
K_F	Freundlich constant (mg/g)
K_L	The adsorption equilibrium constant (L/mg)
K_{RP}	The isothermal adsorption constant in the Redlich-Peterson model (L/g)
n	A parameter in the Freundlich model
p	Probability value
PFO	The pseudo first-order kinetics
PSO	The pseudo second-order kinetics

q_t	The adsorption capacity at time t (mg/g)
q_e	The equilibrium adsorption capacity (mg/g)
q_m	The maximum adsorption capacity (mg/g)
R^2	Coefficient of determination
R-P	The Redlich Peterson isotherm model
SEM	Scanning electron microscope
SSR	Sweet sorghum residue
t	t-value in t -test
TC	Total Cr
XANES	X-ray absorption near edge structure
α	The initial adsorption rate in the Elovich model (mg/(g·h))
β	The desorption constant in the Elovich model (g/mg)
β_{RP}	An index between 0 and 1 in the Redlich-Peterson model

References

- Wang, H.; Xu, J.; Liu, X.; et al. Preparation of straw activated carbon and its application in wastewater treatment: A review. *J. Clean. Prod.* **2021**, *283*, 124671.
- Chen, J.; Cai, Y.; Wang, Z.; et al. Construction of a synthetic microbial community for enzymatic pretreatment of wheat straw for biogas production via anaerobic digestion. *Environ. Sci. Technol.* **2024**, *58*, 9446–9455.
- Tao, W.; Yang, X.; Li, Y.; et al. Components and persistent free radicals in the volatiles during pyrolysis of lignocellulose biomass. *Environ. Sci. Technol.* **2020**, *54*, 13274–13281.
- Zhuo, H.; Dong, X.; Liu, Q.; et al. Bamboo-inspired ultra-strong nanofiber-reinforced composite hydrogels. *Nat. Commun.* **2025**, *16*, 980.
- Hou, D.; Jia, X.; Wang, L.; et al. Global soil pollution by toxic metals threatens agriculture and human health. *Science* **2025**, *388*, 316–321.
- Zhao, K.; Zhang, W.; Liang, Z.; et al. Facilitating new chromium reducing microbes to enhance hexavalent chromium reduction by in situ sonoporation—Mediated gene transfer in soils. *Environ. Sci. Technol.* **2023**, *57*, 15123–15133.
- Thabede, P.M.; Shooto, N.D. Application of black cumin (*Nigella sativa* L.) seeds for the removal of metal ions and methylene blue from aqueous solutions. *Cogent Eng.* **2022**, *9*, 2013419.
- Vinayagam, R.; Dave, N.; Varadavenkatesan, T.; et al. Artificial neural network and statistical modelling of biosorptive removal of hexavalent chromium using macroalgal spent biomass. *Chemosphere* **2022**, *296*, 133965.
- Cho, S.; Jung, S.; Park, J.; et al. Strategic use of crop residue biochars for removal of hazardous compounds in wastewater. *Bioresour. Technol.* **2023**, *387*, 129658.
- Guerin, T.; Ghinet, A.; Hossart, M.; et al. Wheat and ryegrass biomass ashes as effective sorbents for metallic and organic pollutants from contaminated water in lab-engineered cartridge filtration system. *Bioresour. Technol.* **2020**, *318*, 124044.
- Han, F.; An, S.; Liu, L.; et al. Sulfoaluminate cement-modified straw biochar as a soil amendment to inhibit Pb-Cd mobility in the soil-remaine lettuce system. *Chemosphere* **2023**, *332*, 138891.
- Qu, J.; Wang, Y.; Tian, X.; et al. KOH-activated porous biochar with high specific surface area for adsorptive removal of chromium (VI) and naphthalene from water: Affecting factors, mechanisms and reusability exploration. *J. Hazard. Mater.* **2021**, *401*, 123292.
- Tian, S.; Shu, X.; Jiang, X.; et al. Mineralization and stabilization of toxic Pb^{2+} ions using CMC loaded S/P co-doped biochar composite. *Sep. Purif. Technol.* **2025**, *354*, 129161.
- Wu, Y.; Ming, J.; Zhou, W.; et al. Efficiency and mechanism in preparation and heavy metal cation/anion adsorption of amphoteric adsorbents modified from various plant straws. *Sci. Total Environ.* **2023**, *884*, 163887.
- Gkika, D.A.; Tolkou, A.K.; Katsoyiannis, I.A.; et al. The adsorption-desorption-regeneration pathway to a circular economy: The role of waste-derived adsorbents on chromium removal. *Sep. Purif. Technol.* **2025**, *368*, 132996.
- Rzig, B.; Guesmi, F.; Sillanpaa, M.; et al. Biosorption potential of olive leaves as a novel low-cost adsorbent for the removal of hexavalent chromium from wastewater. *Biomass Convers. Biorefinery* **2024**, *14*, 12961–12979.
- Zhen, H.G.; Hu, C.; Yang, L.; et al. Hydrochar produced from mixed feedstocks as efficient adsorbent for selenium and chromium removal from acidic wastewater. *Desalination* **2025**, *593*, 118152.
- Paglizccia, B.; Carretti, E.; Severi, M.; et al. Heavy metal biosorption by Extracellular Polymeric Substances (EPS) recovered from anammox granular sludge. *J. Hazard. Mater.* **2022**, *424*, 126661.
- Ubando, A.T.; Africa, A.D.M.; Maniquiz-Redillas, M.C.; et al. Microalgal biosorption of heavy metals: A comprehensive bibliometric review. *J. Hazard. Mater.* **2021**, *402*, 123431.
- Wang, J.L.; Chen, C. Biosorbents for heavy metals removal and their future. *Biotechnol. Adv.* **2009**, *27*, 195–226.
- Wang, P.; Yue, F.; Shao, C.; et al. Bio-sorption capacity of cadmium and zinc by *Pseudomonas monteili* with heavy-metal resistance isolated from the compost of pig manure. *Bioresour. Technol.* **2024**, *399*, 130589.

22. Miretzky, P.; Cirelli, A.F. Cr(VI) and Cr(III) removal from aqueous solution by raw and modified lignocellulosic materials: A review. *J. Hazard. Mater.* **2010**, *180*, 1–19.
23. Ifthikar, J.; Zhao, M.; Shahzad, A.; et al. Recyclable process modeling study of hexavalent chromium elimination by thiol-based electron donor: Implications for practical applicability. *J. Environ. Chem. Eng.* **2021**, *9*, 105645.
24. Kim, K.; Chung, H.Y.; Kim, B.; et al. Freezing-induced simultaneous reduction of chromate and production of molecular iodine: Mechanism, Kinetics, and practical Implications. *Environ. Sci. Technol.* **2020**, *54*, 16204–16211.
25. Krishnani, K.K.; Meng, X.; Christodoulatos, C.; et al. Biosorption mechanism of nine different heavy metals onto biomatrix from rice husk. *J. Hazard. Mater.* **2008**, *153*, 1222–1234.
26. Liang, J.; Zhen, P.; Liu, L.; et al. Functional group-specific reduction of Cr(VI) by low molecular weight organic acids in frozen solution: Kinetics, mechanism and DFT calculation. *Water Res.* **2024**, *265*, 122221.
27. Wang, W.; Fang, X.; Fu, Q.; et al. Iron(II/III) alters the relative roles of the microbial byproduct and humic acid during chromium(VI) reduction and fixation by soil-dissolved organic matter. *Environ. Sci. Technol.* **2025**, *59*, 2778–2790.
28. Li, S.Z.; Chan-Halbrendt, C. Ethanol production in (the) People's Republic of China: Potential and technologies. *Appl. Energy* **2009**, *86*, S162–S169.
29. Wu, J.; Dong, J.; Wang, J. Adsorptive removal of Cu(II) from aqueous solution by fermented sweet sorghum residues as a novel biosorbent. *J. Mol. Liq.* **2022**, *367*, 120362.
30. Wang, J.L.; Guo, X. Adsorption kinetic models: Physical meanings, applications, and solving methods. *J. Hazard. Mater.* **2020**, *390*, 122156.
31. Wang, J.L.; Guo, X. Rethinking of the intraparticle diffusion adsorption kinetics model: Interpretation, solving methods and applications. *Chemosphere* **2022**, *309*, 136732.
32. Wang, J.L.; Guo, X. Adsorption isotherm models: Classification, physical meaning, application and solving method. *Chemosphere* **2020**, *258*, 127279.
33. Wang, J.L.; Guo, X. Adsorption kinetics and isotherm models of heavy metals by various adsorbents: An overview. *Crit. Rev. Environ. Sci. Technol.* **2023**, *53*, 1837–1865.
34. Richard, F.C.; Bourg, A.C.M. Aqueous geochemistry of chromium: A review. *Water Res.* **1991**, *25*, 807–816.
35. Foday, E.H.; Bo, B.; Xu, X. Removal of toxic heavy metals from contaminated aqueous solutions using seaweeds: A review. *Sustainability* **2021**, *13*, 12311.
36. Verma, R.; Maji, P.K.; Sarkar, S. Comprehensive investigation of the mechanism for Cr(VI) removal from contaminated water using coconut husk as a biosorbent. *J. Clean. Prod.* **2021**, *314*, 128117.